Multiplicity of stable orbits for deformable prolate capsules in shear flow

Xiao Zhang and Michael D. Graham ⓘ*

*Department of Chemical and Biological Engineering, University of Wisconsin-Madison,
Madison, Wisconsin 53706-1691, USA*

This work investigates the orbital dynamics of a fluid-filled deformable prolate capsule in unbounded simple shear flow at zero Reynolds number using direct simulations. The motion of the capsule is simulated using a model that incorporates shear elasticity, area dilatation, and bending resistance. Here the deformability of the capsule is characterized by the nondimensional capillary number Ca, which represents the ratio of viscous stresses to elastic restoring stresses on the capsule. For a capsule with small bending stiffness, at a given Ca, the orientation converges over time toward a unique stable orbit independent of the initial orientation. With increasing Ca, four dynamical modes are found for the stable orbit, namely rolling, wobbling, oscillating-swinging, and swinging. On the other hand, for a capsule with large bending stiffness, multiplicity in the orbit dynamics is observed. When the viscosity ratio $\lambda \lesssim 1$, the long axis of the capsule always tends toward a stable orbit in the flow-gradient plane, either tumbling or swinging, depending on Ca. When $\lambda \gtrsim 1$, the stable orbit of the capsule is a tumbling motion at low Ca, irrespective of the initial orientation. Upon increasing Ca, there is a symmetry-breaking bifurcation away from the tumbling orbit, and the capsule is observed to adopt multiple stable orbital modes including nonsymmetric precessing and rolling, depending on the initial orientation. As Ca increases further, the nonsymmetric stable orbit loses existence at a saddle-node bifurcation, and rolling becomes the only attractor at high Ca, whereas the rolling state coexists with the nonsymmetric state at intermediate values of Ca. A symmetry-breaking bifurcation away from the rolling orbit is also found upon decreasing Ca. The regime with multiple attractors becomes broader as the aspect ratio of the capsule increases, while it narrows as the viscosity ratio increases. We also report the particle contribution to the stress, which also displays multiplicity.

I. INTRODUCTION

Microcapsules, small liquid droplets enclosed by a thin solid membrane, have been of increasing significance in the bioengineering, pharmaceutics, and food industries. Examples include cell encapsulation for tumor progression monitoring [1], encapsulation of cosmetic active ingredients for topical application [2], development of drug delivery systems [3,4], and artificial food particles for aquatic filter feeders [5].

To satisfy engineering needs, many fabrication techniques for artificial capsules have emerged. Polyelectrolyte capsules (PECs), for example, are a promising vehicle in the biomedical field to carry a variety of therapeutic molecules (peptides, proteins, etc.) for targeted delivery to a desired site in the body [6]. Avoidance of immune clearance (cellular uptake by macrophages), which is critical for the efficiency of carrier particles in a delivery system, has been revealed to

---

*Author to whom all correspondence should be addressed: mdgraham@wisc.edu

greatly depend on particle physical and chemical properties such as size, shape, deformability, and surface chemistry. A number of studies have reported that high-aspect-ratio (prolate) microparticles exhibited considerably reduced immune clearance and increased circulation half-time compared to spheres [7,8]. To this end, Zan *et al.* [9] developed a fabrication method to obtain PECs with constant surface chemistry but independently controlled size and shape by combining soft organic templates created by the particle stretching method and a modified layer-by-layer (LBL) deposition process, which may enable both a more systematic investigation of the roles of capsule properties on its efficiency, and the optimization of the design of a delivery system. Furthermore, nonspherical capsules, because of a higher surface-to-volume ratio than their spherical counterparts, can be preferable to enhance the transfer of cargoes across the capsule membrane upon arrival at the target; an example is the fabrication of prolate capsules containing a calcium ion solution by Schneeweiss and Rehage [10] using a microfluidic channel.

All of the aforementioned situations involve capsule suspensions in a fluid environment, and the dynamics of these suspensions can be greatly affected by the behavior of single capsules. Therefore, it is essential to gain a comprehensive understanding of the single capsule dynamics in a flow. For example, an initially spherical deformable capsule is found to take a so-called tank-treading motion in simple shear flow with the membrane rotating periodically around its stationary elongated shape [11]. Here the deformability of the capsule is characterized by the capillary number Ca, which represents the ratio of viscous stresses to elastic restoring stresses on the particle. Nonspherical capsules, such as oblate spheroids [12–22] and biconcave discoids, a model for red blood cells (RBCs) [23–35], have also been investigated extensively in both experimental and computational studies. These studies have explored a wide range of parameters for the capsule membrane mechanics and flow properties, and revealed rich and complex orbital dynamics for the capsules. Indeed, the increasing attention that oblate capsules have gained in the past decades may be attributed to the findings by several studies on RBCs [32–35] showing that an oblate spheroidal spontaneous shape has to be assumed for RBCs to maintain the stability of their biconcave shape during motions, and it provides a better prediction than other spontaneous shapes for cell dynamics in comparison with experimental observations.

In contrast, to the best of our knowledge, there only exist a limited number of works on the motion of prolate capsules in shear flow, most of which have focused on the special case where the fluids inside and outside the capsules have the same viscosity. Walter *et al.* [17] numerically studied the motion of an inertialess prolate capsule in shear flow with the major axis initially positioned in the shear plane. The membrane was modeled as a thin hyperelastic surface with no bending resistance. Two stable in-plane orbital motions were found: a rigid-body-like tumbling motion at low Ca, in which the capsule flips continuously, and a fluidlike motion named swinging at high Ca, which is similar to a tank-treading motion only with small oscillations in both the deformation and orientation of the capsule. Richer orbital dynamics have been revealed for a prolate capsule with out-of-shear-plane initial orientations. In a numerical investigation by Dupont *et al.* [36], the membrane mechanics of the capsule was described using a model that includes shear elasticity and area dilatation described by either the Skalak law [37] or the neo-Hookean law, but again no bending resistance. They showed that for any initial orientation with respect to the vorticity axis, the capsule always converges toward a unique stable long-time orbit depending on Ca. At low Ca, the stable orbit corresponds to a rolling motion about the vorticity axis. As Ca increases, the capsule precesses around the vorticity axis, and undergoes a so-called wobbling motion. At high Ca, the capsule assumes a complex motion with oscillations about the shear plane termed oscillating-swinging, which eventually evolves into a swinging motion, as described in [17], as Ca further increases. The same qualitative motions were generally observed in the parameter regimes considered in this work, irrespective of the capsule membrane law or aspect ratio. Cordasco and Bagchi [20] later incorporated a small constant bending stiffness into the membrane for an inertialess prolate capsule with zero spontaneous curvature, and observed a transition of the stable orbit from a drift precession (rolling) to a stable precession with a tank-treading motion of the membrane (oscillating-swinging) as Ca increases, which is qualitatively similar to the observations in [36].
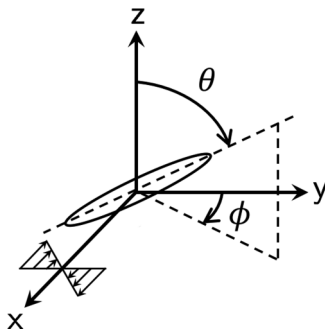
FIG. 1. Schematic of the 3D orientation of a prolate capsule in unbounded simple shear flow.

The effect of a small particle inertia was considered by Wang *et al.* [21] for the three-dimensional orbital behavior of an isolated prolate capsule in shear flow, in which, again, bending resistance was neglected and a unity viscosity ratio between the inner and outer fluids was assumed. With increasing Ca, the dominant stable orbital modes were found to be tumbling, precessing, rolling, and oscillating-swinging. In contrast to the findings in [36] and [20], they revealed that multiple stable orbits coexist in the transition regimes, even at the same capillary number.

None of the preceding studies regarding deformable prolate capsules have addressed the effects of bending stiffness and viscosity ratio, which may both play a nontrivial role in the orbital dynamics of the capsules. In fact, in applications, the mechanical properties of the capsule membrane can vary greatly depending on the materials and fabrication techniques, and the suspending fluid or solution and the fluid enclosed inside the capsules will generally have different viscosities. The present work aims to gain an improved understanding of the dynamics of prolate capsules in shear flow by performing a systematic numerical investigation over a broad domain of parameter space and determining the effects of membrane deformability, bending stiffness, initial orientation, the aspect ratio of the capsule, and the viscosity ratio between the inner and outer fluids. In this work, we reveal parameter regimes for an inertialess deformable prolate capsule in shear flow in which either a single or multiple attractors exist, and we show in particular that the orbits for a capsule lying in the shear plane and aligned with the vorticity axis are not always stable as the capsule evolves toward the equilibrium configuration. By computing the particle contribution to the stress, we illustrate how the multiplicity of stable orbits for a prolate capsule is reflected in the rheology for a suspension of such capsules in the dilute limit. The connection between orbit dynamics and rheology for capsules has been reported in a number of prior studies [12,38–45], but only a small number have considered prolate capsules.

The rest of the paper is organized as follows: in Sec. II we present the models for a deformable prolate capsule and the membrane mechanics, and the numerical method adopted to calculate the fluid motion; in Sec. III we provide detailed results and discussion for the orbital dynamics of a prolate capsule over a broad range of various parameters, including membrane deformability, bending stiffness, initial orientation, the aspect ratio of the capsule, and the viscosity ratio between the inner and outer fluids. Predictions of the rheological properties for a dilute suspension of prolate capsules are also reported. Concluding remarks are presented in Sec. IV.

II. MODEL FORMULATION

A. Model and discretization

We consider an isolated inertialess fluid-filled deformable capsule with a prolate spheroidal rest shape immersed in unbounded simple shear flow with shear rate $\dot{\gamma}$ (Fig. 1). The undisturbed flow velocity is given by $\mathbf{u}^\infty = (\dot{\gamma}y, 0, 0)$. Both the suspending fluid and the fluid inside the capsule are assumed to be incompressible and Newtonian, with viscosity η and $\lambda\eta$, respectively, where λ is the

viscosity ratio. At rest, the prolate capsule has a polar radius a_1 and an equatorial radius a_2, with an aspect ratio $\text{AR} = a_1/a_2 > 1$. Here we define a characteristic length scale $a = (a_1 a_2^2)^{1/3}$; this is the radius of a sphere having the same volume as the prolate capsule. The particle Reynolds number $\text{Re}_p = \rho\dot{\gamma}a^2/\eta$ is assumed to be sufficiently small so that the fluid motion is governed by the Stokes equation. The instantaneous orientation of the prolate capsule is given by two angles, as defined by Jeffery [46]: ϕ is the azimuthal angle with respect to the y axis, and θ is the polar angle with respect to the z axis.

To describe the membrane mechanics, we adopt a model that incorporates shear elasticity, area dilatation, and bending resistance. The total energy E of the capsule membrane S is given as

$$E = \frac{K_B}{2}\int_S (2\kappa_H + c_0)^2 dS + \overline{K_B}\int_S \kappa_G dS + \int_S W\, dS, \tag{1}$$

where K_B and $\overline{K_B}$ are the bending moduli, and W is the shear strain energy density; κ_H and κ_G are the mean and Gaussian curvature of the membrane surface, respectively; $c_0 = -2H_0$ is the spontaneous curvature, H_0 being the mean curvature of the spontaneous shape. In this equation, the first two terms represent the Canham-Helfrich bending energy [47,48], and the third term corresponds to the shear strain energy. The behavior of the capsule membrane in response to the in-plane shear elastic force is described using a membrane model by Skalak $et\ al.$ [37], in which the shear strain energy density W is given by

$$W_{\text{SK}} = \frac{G}{4}\big[(I_1^2 + 2I_1 - 2I_2) + C_a I_2^2\big], \tag{2}$$

where G is the in-plane shear modulus of the membrane, and C_a characterizes the energy penalty for the area change of the membrane. The strain invariants I_1 and I_2 are functions of the principal stretch ratios λ_1 and λ_2, defined as

$$I_1 = \lambda_1^2 + \lambda_2^2 - 2, \quad I_2 = \lambda_1^2 \lambda_2^2 - 1. \tag{3}$$

Barthès-Biesel $et\ al.$ [49] showed that for $C_a \gtrsim 10$, the tension of a Skalak membrane becomes nearly independent of C_a under a simple uniaxial deformation, so C_a is set to 10 for all of the simulations in the present work. The deformability and bending stiffness of the capsule are characterized by the dimensionless capillary number $\text{Ca} = \eta\dot{\gamma}a/G$ and bending modulus $\hat{\kappa}_B = K_B/a^2 G$, respectively. Taking the first variation of the total membrane energy E in Eq. (1) gives the total membrane strain force density:

$$\mathbf{f^m} = \mathbf{f^b} + \mathbf{f^s}, \tag{4}$$

where $\mathbf{f^b}$ and $\mathbf{f^s}$ are bending and shear elastic force densities, respectively. Note that according to the Gauss-Bonnet theorem, the second term in Eq. (1), i.e., the term involving the Gaussian curvature κ_G, is a constant when no topological changes are involved, so there is no force density associated with that term [20]. Hence, the force density due to bending resistance is given by the first variation of only the first term in Eq. (1).

The capsule membrane is discretized into 320 piecewise flat triangular elements, resulting in 162 nodes. We have verified that increasing the number of membrane elements from 320 to 1280 makes no difference to the orbital dynamics of capsules with varying bending stiffness and viscosity ratio. Based on this discretization, the calculation of the total membrane force density $\mathbf{f^m}$ follows the work of Kumar and Graham [50] and Sinha and Graham [35] using approaches given by Charrier $et\ al.$ [51] for the in-plane shear force density $\mathbf{f^s}$ and Meyer $et\ al.$ [52] for the out-of-plane bending force density $\mathbf{f^b}$, respectively. Details regarding these calculations are found in [50] and [35].

B. Fluid motion

In the Stokes flow regime, the fluid velocity $\mathbf{u}$ at any point $\mathbf{x_0}$ in the unbounded domain can be written in boundary integral form [50,53] as

$$u_j(\mathbf{x_0}) = u_j^\infty(\mathbf{x_0}) + \int_S q_i(\mathbf{x})G_{ji}(\mathbf{x_0}, \mathbf{x})dS(\mathbf{x}), \tag{5}$$

where $\mathbf{q}(\mathbf{x_0})$ is a single-layer density that satisfies

$$q_j(\mathbf{x_0}) + \frac{\lambda - 1}{4\pi(\lambda + 1)}n_k(\mathbf{x_0})\int_S q_i(\mathbf{x})T_{jik}(\mathbf{x_0}, \mathbf{x})dS(\mathbf{x}) = -\frac{1}{4\pi\mu}\left(\frac{\Delta f_j(\mathbf{x_0})}{\lambda + 1} + \frac{\lambda - 1}{\lambda + 1}f_j^\infty(\mathbf{x_0})\right). \tag{6}$$

Here $\mathbf{u}^\infty(\mathbf{x_0})$ is the undisturbed fluid velocity at a given point $\mathbf{x_0}$; S denotes the surface of the particle; $\mathbf{f}^\infty(\mathbf{x_0})$ is the traction at a given point due to the stress generated in the fluid corresponding to the undisturbed flow $\mathbf{u}^\infty(\mathbf{x_0})$; $\Delta\mathbf{f}(\mathbf{x})$ is the hydrodynamic traction jump across the membrane interface, which relates to the total membrane force density by $\Delta\mathbf{f}(\mathbf{x}) = -\mathbf{f^m}$ assuming the membrane equilibrium condition; and $\mathbf{G}$ and $\mathbf{T}$ are the Green's function and its associated stress tensor for Stokes flow in an unbounded domain. Details of the numerical method are described in [50]. Once the flow field is determined, the positions of the element nodes on the discretized capsule membrane are advanced in time using a second-order Adams-Bashforth method with adaptive time step $\Delta t = 0.02\mathrm{Ca}l$, where l is the minimum node-to-node distance. Time is nondimensionalized by the shear rate $\dot{\gamma}$, and in this work we define t as the dimensionless time.

The implementation of the boundary integral method used in this work has been extensively validated with test problems considering both a rigid sphere and a spherical drop between parallel walls subjected to pressure-driven flow, and the numerical algorithms applied to calculate the shear and bending elastic force densities in the capsule membrane have been validated on the deformation of spherical capsules in simple shear flow. We have also compared the numerically determined inclination profile for a highly stiff prolate capsule with the prediction by Jeffery's theory [46] for an inertialess rigid prolate particle in shear flow, and we observed good agreement. See [35,50,54] for details.

C. Particle stress in a dilute suspension of capsules

In addition to the capsule motions, we also compute the particle stress tensor in order to understand the rheology for a suspension of such capsules in the dilute limit. For a suspension of N_p capsules in a volume V, the contribution of the suspended capsules to the bulk stress of the suspension, in dimensional form, is given by [12,42,55–57]

$$\Sigma_{ij}^p = \frac{1}{V}\sum_{m=1}^{N_p}\int_{S_m}[\Delta f_i x_j + \eta(\lambda - 1)(u_i n_j + u_j n_i)]dS, \tag{7}$$

where $\mathbf{\Sigma^p}$ is the particle stress tensor. Rewritten in nondimensional variables, $\widetilde{\mathbf{x}} = \mathbf{x}/a$, $\widetilde{\mathbf{u}} = \mathbf{u}/(a\dot{\gamma})$, $\widetilde{V} = V/a^3$, $\widetilde{S} = S/a^2$, and $\widetilde{\Delta\mathbf{f}} = \Delta\mathbf{f}/(\eta\dot{\gamma})$, Eq. (7) becomes

$$\Sigma_{ij}^p = \frac{\eta\dot{\gamma}}{\widetilde{V}}\sum_{m=1}^{N_p}\int_{\widetilde{S}_m}[\widetilde{\Delta f_i}\widetilde{x}_j + (\lambda - 1)(\widetilde{u}_i n_j + \widetilde{u}_j n_i)]d\widetilde{S}. \tag{8}$$

Now we assume that the suspension is dilute, containing N_p identical prolate capsules all undergoing the same stable orbital motion, and that the interparticle hydrodynamic interactions are negligible. The volume fraction of the suspension is given by $\Phi = N_p V_p/V = N_p\widetilde{V}_p/\widetilde{V}$, where V_p is the volume
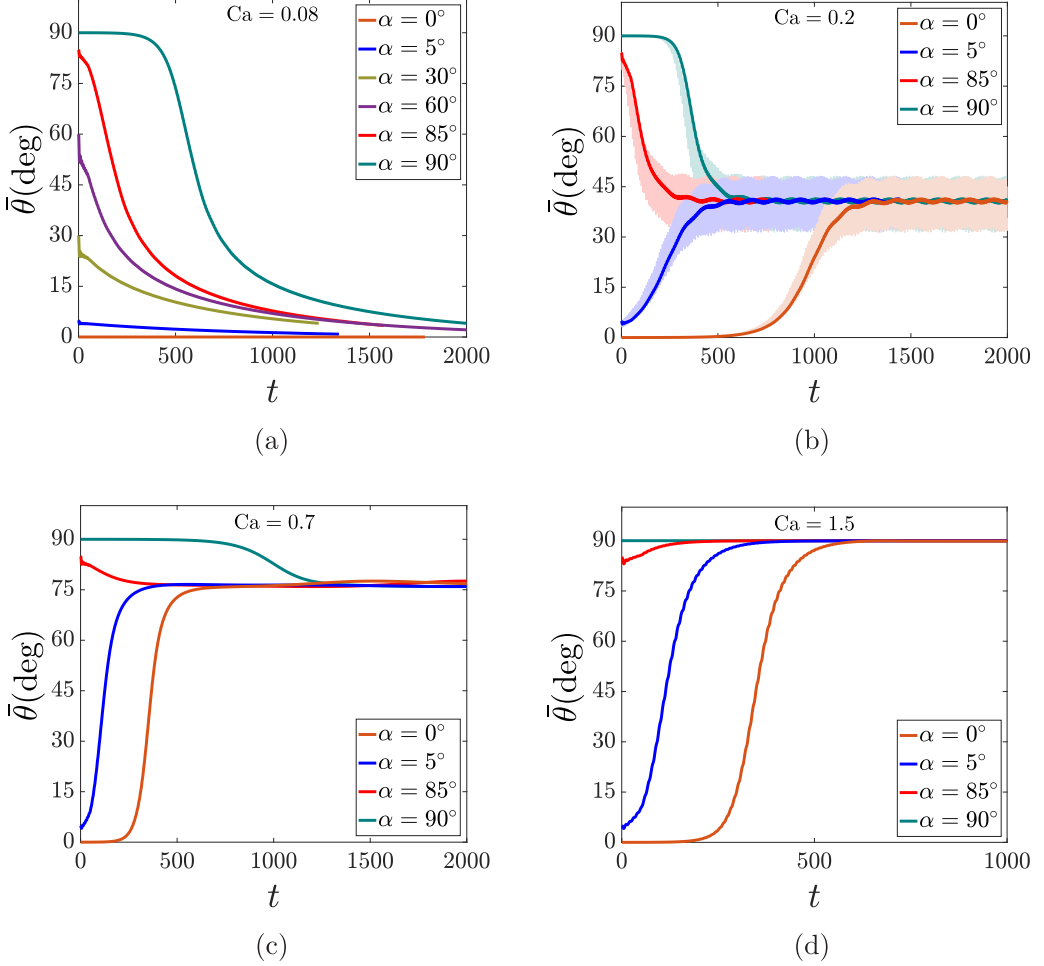
FIG. 2. Evolution of $\bar{\theta}$ of a prolate capsule (AR = 2.0) with $\hat{\kappa}_B = 0.02$ and $\lambda = 1$ at (a) Ca = 0.08, (b) Ca = 0.2, (c) Ca = 0.7, and (d) Ca = 1.5. Here the spontaneous shape of the capsule is assumed to be the same as its rest shape.

of a single capsule and $\widetilde{V}_p = V_p/a^3$ is dimensionless. Equation (8) now becomes

$$\Sigma_{ij}^p = \frac{\eta\dot{\gamma}N_p}{\widetilde{V}} \int_{\widetilde{S}_m} [\widetilde{\Delta f_i}\widetilde{x}_j + (\lambda - 1)(\widetilde{u}_i n_j + \widetilde{u}_j n_i)]d\widetilde{S}$$

$$= \frac{\eta\dot{\gamma}\,\Phi}{\widetilde{V}_p} \int_{\widetilde{S}_m} [\widetilde{\Delta f_i}\widetilde{x}_j + (\lambda - 1)(\widetilde{u}_i n_j + \widetilde{u}_j n_i)]d\widetilde{S}, \tag{9}$$

which naturally gives the dimensionless particle stress tensor

$$\widetilde{\Sigma}_{ij}^p = \frac{\Sigma_{ij}^p}{\eta\dot{\gamma}} = \frac{\Phi}{\widetilde{V}_p} \int_{\widetilde{S}_m} [\widetilde{\Delta f_i}\widetilde{x}_j + (\lambda - 1)(\widetilde{u}_i n_j + \widetilde{u}_j n_i)]d\widetilde{S}. \tag{10}$$

The dimensionless particle shear stress $\widetilde{\Sigma}_{xy}^p$ is identical to the specific viscosity η_{sp}; for a dilute suspension of rigid spherical particles, $\eta_{sp} = [\eta]\Phi = 2.5\Phi$ [58], where $[\eta]$ is the intrinsic viscosity.
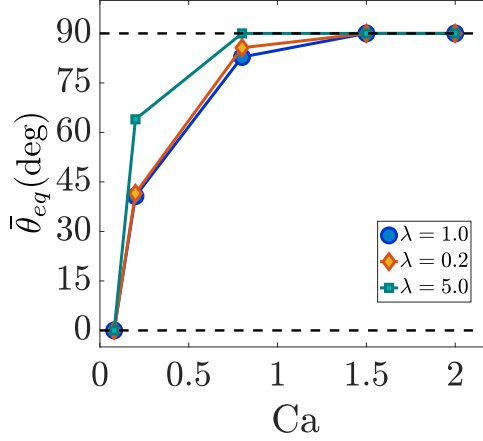
FIG. 3. Bifurcation behavior for a prolate capsule (AR = 2.0) with $\hat{\kappa}_B = 0.02$ and varying λ. The black dashed lines at $\theta = 0°$ and $90°$ represent the orbits for a capsule aligned with the z axis and in the shear plane, respectively.

The dimensionless first and second normal stress differences are $N_1 = \widetilde{\Sigma^p_{xx}} - \widetilde{\Sigma^p_{yy}}$ and $N_2 = \widetilde{\Sigma^p_{yy}} - \widetilde{\Sigma^p_{zz}}$.

III. RESULTS AND DISCUSSION

In this section, the orbital dynamics of a prolate capsule in unbounded simple shear flow are systematically investigated over a broad domain of parameter space. We focus on addressing the issue of long-time behavior of the orbits. For a capsule with small bending stiffness (Sec. III A), all initial conditions we consider evolve toward the same orbit at long times. For a capsule with large bending stiffness (Sec. III B), in contrast, we reveal parameter regimes with multiple attractors, i.e., there are multiple stable orbits, and which one is reached at long times depends on the initial orientation. A corresponding multiplicity in the rheological properties is predicted for a dilute suspension of such capsules.

A. Dynamics of prolate capsules with small bending stiffness

We first report the dynamics of a deformable prolate capsule with small bending stiffness ($\hat{\kappa}_B = 0.02$). The initial orientation of the capsule is set to $[\phi^0, \theta^0] = [\pi/2, \alpha]$. We begin with the case where $\lambda = 1$ and AR = 2.0, and we assume that the spontaneous shape of the capsule is the same as its rest shape. The effect of spontaneous curvature will be discussed later. Figure 2 shows the evolution of the capsule orbit in various regimes of Ca. We are interested in the long-time limit (dimensionless time $t \gg 1$) of the capsule dynamics, so the evolution data are presented using a running average of θ, defined as $\bar{\theta} = \frac{1}{t_{avg}} \int_{t-t_{avg}}^{t} \theta(t)dt$, that averages over the oscillations in θ caused by the rotational motions of the capsule on the time scale $1/\dot{\gamma}$. Here we set $t_{avg} = 50$; Fig. 2(b) shows an example of the evolution data before (light-colored "clouds") and after (solid colored lines) taking the running average.

The key observation here is that the capsule, irrespective of the initial orientation α, evolves toward the same orbit at long times, denoted as $\bar{\theta}_{eq}$. In Fig. 2(a) (Ca = 0.08), six values of α are considered, and the orbit of the capsule always converges toward $\bar{\theta}_{eq} = 0°$. For simplicity, results are only shown for four values of α in Figs. 2(b), 2(c), and 2(d). As Ca increases, $\bar{\theta}_{eq}$ increases from $0°$ to $90°$. This trend holds qualitatively for $\lambda = 0.2$ and 5, and also as AR increases from 2.0 to 3.0 (not shown). The dependence of $\bar{\theta}_{eq}$ on Ca for a prolate capsule (AR = 2.0) with $\hat{\kappa}_B = 0.02$ is
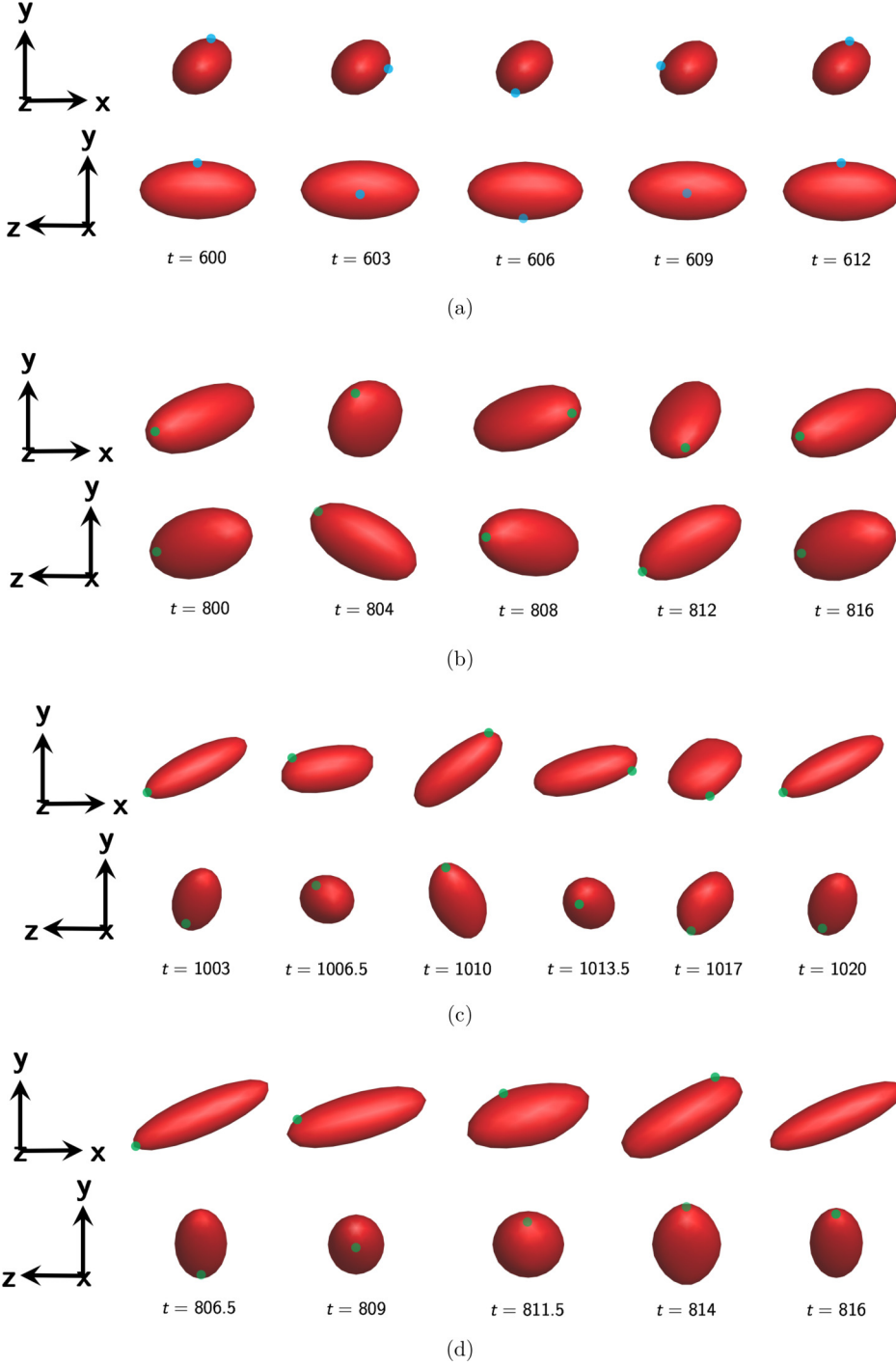
FIG. 4. Time sequence images (side and front views) of a prolate capsule (AR = 2.0) with $\hat{\kappa}_B = 0.02$ and $\lambda = 1$ taking a rolling [(a) Ca = 0.08], wobbling [(b) Ca = 0.2], oscillating-swinging [(c) Ca = 0.7], and swinging [(d) Ca = 1.5] motion, respectively. The initial orientation of the capsule is $\alpha = 5°$. The markers indicate the positions of a membrane point initially on the equator of the capsule for (a), and a membrane point initially on the major axis of the capsule for (b), (c), and (d).
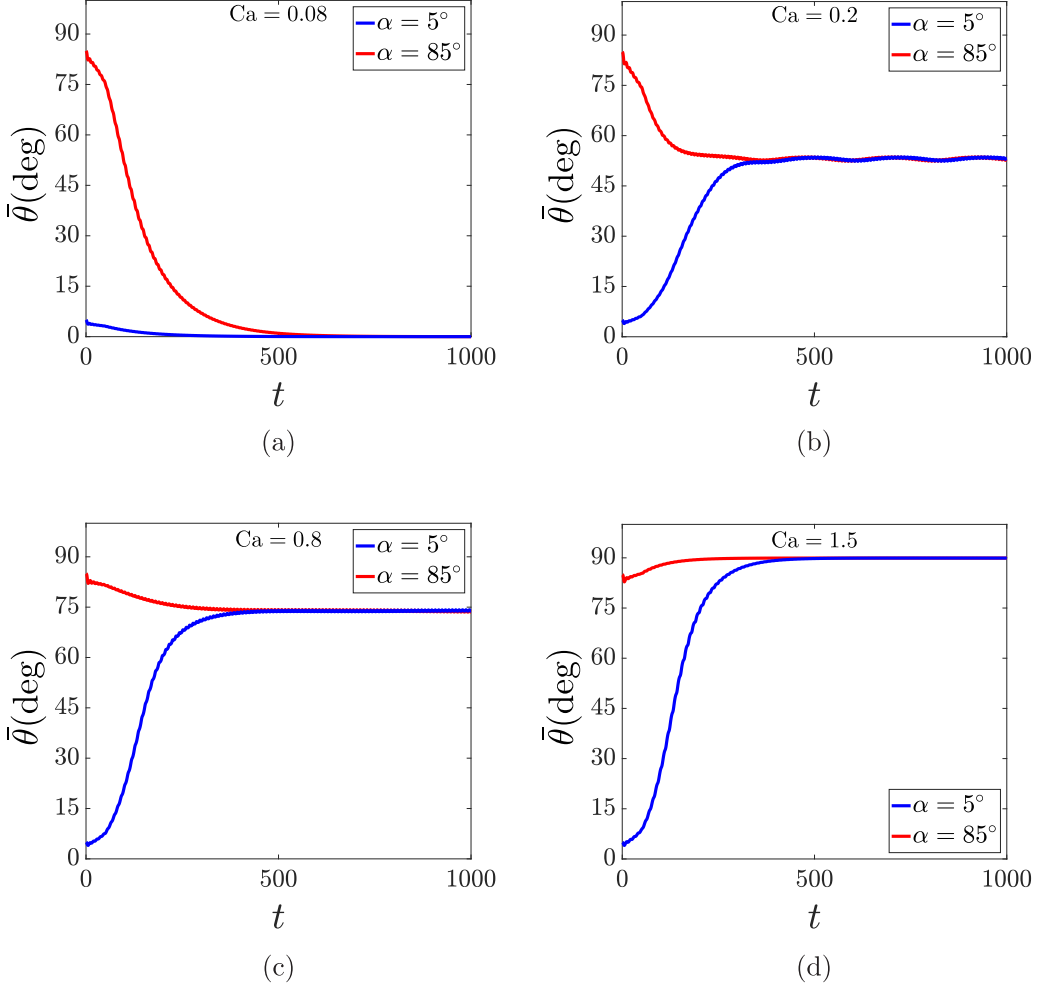
FIG. 5. Evolution of $\bar{\theta}$ of a prolate capsule (AR $= 2.0$) with $\hat{\kappa}_B = 0.02$ and $\lambda = 1$ at (a) Ca $= 0.08$, (b) Ca $= 0.2$, (c) Ca $= 0.8$, and (d) Ca $= 1.5$. Here the spontaneous curvature is assumed to be zero ($c_0 = 0$) everywhere on the membrane surface.

illustrated in a bifurcation diagram with varying λ, as shown in Fig. 3. Note that by symmetry, the orbits for a capsule lying in the shear plane ($\theta = 90°$) and aligned with the z axis ($\theta = 0°$) are always solutions for all parameter values. However, these two solutions may not be stable with respect to symmetry-breaking perturbations; indeed, in the case of $\lambda = 1$ (solid blue line with circles), for example, there is a symmetry-breaking bifurcation away from $\theta = 0°$ between Ca $= 0.08$ and 0.2, and another one away from $\theta = 90°$ between Ca $= 0.7$ and 1.5.

We now look into the detailed motions of the capsule in different Ca regimes. With increasing Ca, four orbital modes are determined corresponding to the stable orbits in different regimes. At very low Ca, the major axis of the capsule is observed to evolve toward the vorticity axis via a process termed drifting precession [20], until the capsule takes a stable rolling motion [Fig. 4(a)]. As Ca increases, the capsule orbit drifts toward an intermediate equilibrium configuration where the capsule exhibits a wobbling behavior while precessing about the vorticity axis [Fig. 4(b)]; this motion is named stable precession in [20]. In the regime of higher Ca, the capsule adopts a complex motion termed oscillating-swinging [Fig. 4(c)], in which the long axis of the elongated capsule oscillates both about the shear plane and about a mean inclination with respect to the flow direction,
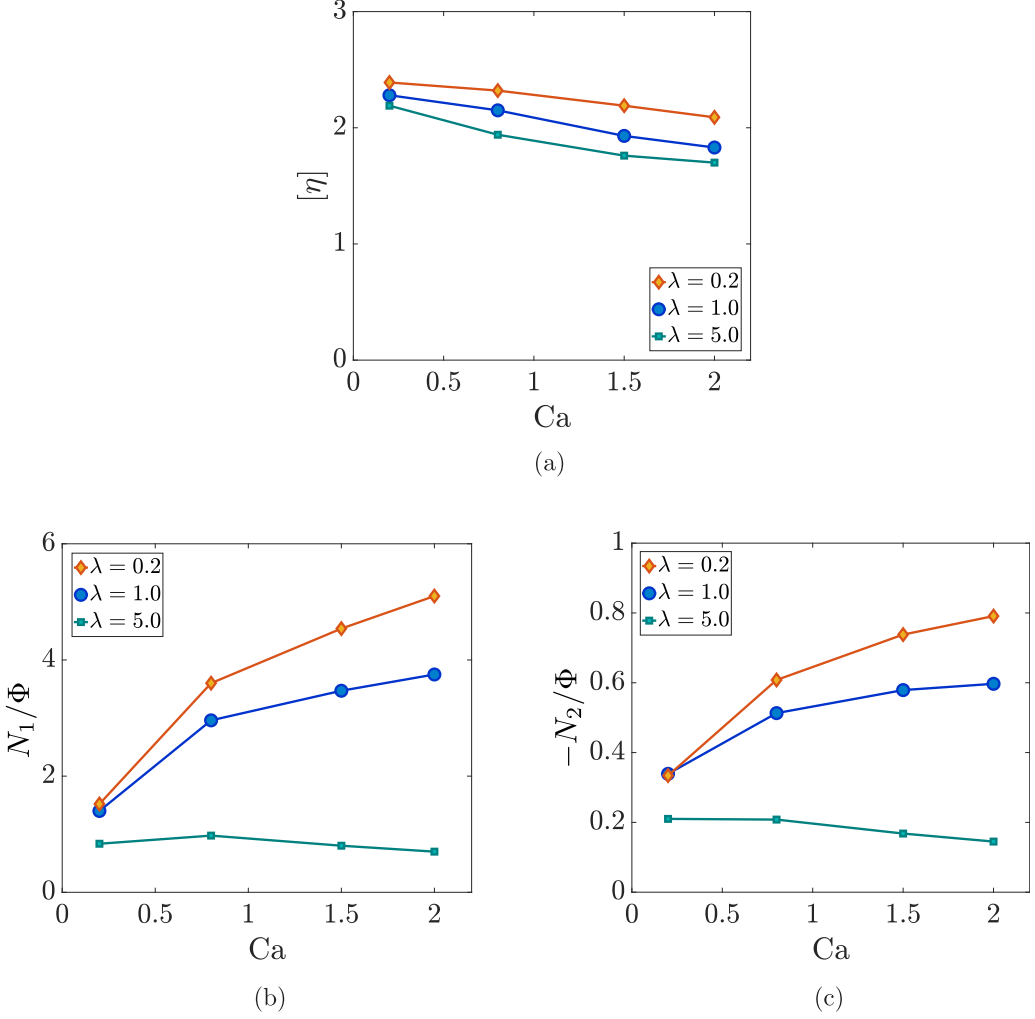
FIG. 6. Intrinsic viscosity (a) and dimensionless normal stress differences (b,c) predicted for a dilute suspension (with volume fraction Φ) of identical prolate capsules (AR $= 2.0$) with $\hat{\kappa}_B = 0.02$ taking the same corresponding stable orbit at varying Ca.

while the membrane of the capsule rotates around its deformed shape with the capsule elongation oscillating over time, as described by Dupont *et al.* [36]. With a further increase in Ca [Fig. 4(d)], the oscillations about the shear plane in the oscillating-swinging motion vanish, and a pure in-plane fluidlike swinging motion, as described by Walter *et al.* [17], is assumed eventually. This qualitative transition of stable orbital motions for a prolate capsule agrees well with the findings by Dupont *et al.* [36], which did not include bending resistance.

In addition, we examine the effect of spontaneous curvature on the orbital dynamics of the prolate capsule. Figure 5 shows the orbit evolution for a capsule with zero spontaneous curvature ($c_0 = 0$) everywhere on the membrane surface. For each Ca, the long-time orbit is independent of the initial orientation, and thus only the results for $\alpha = 5°$ and $85°$ are shown here. Similar to the previous case, $\bar{\theta}_{eq}$ is observed to increase from $0°$ to $90°$ at increasing Ca. Same stable motion modes are determined, namely rolling, wobbling, oscillating-swinging, and swinging, associated with different Ca regimes. Cordasco and Bagchi [20] also found a qualitatively similar transition of
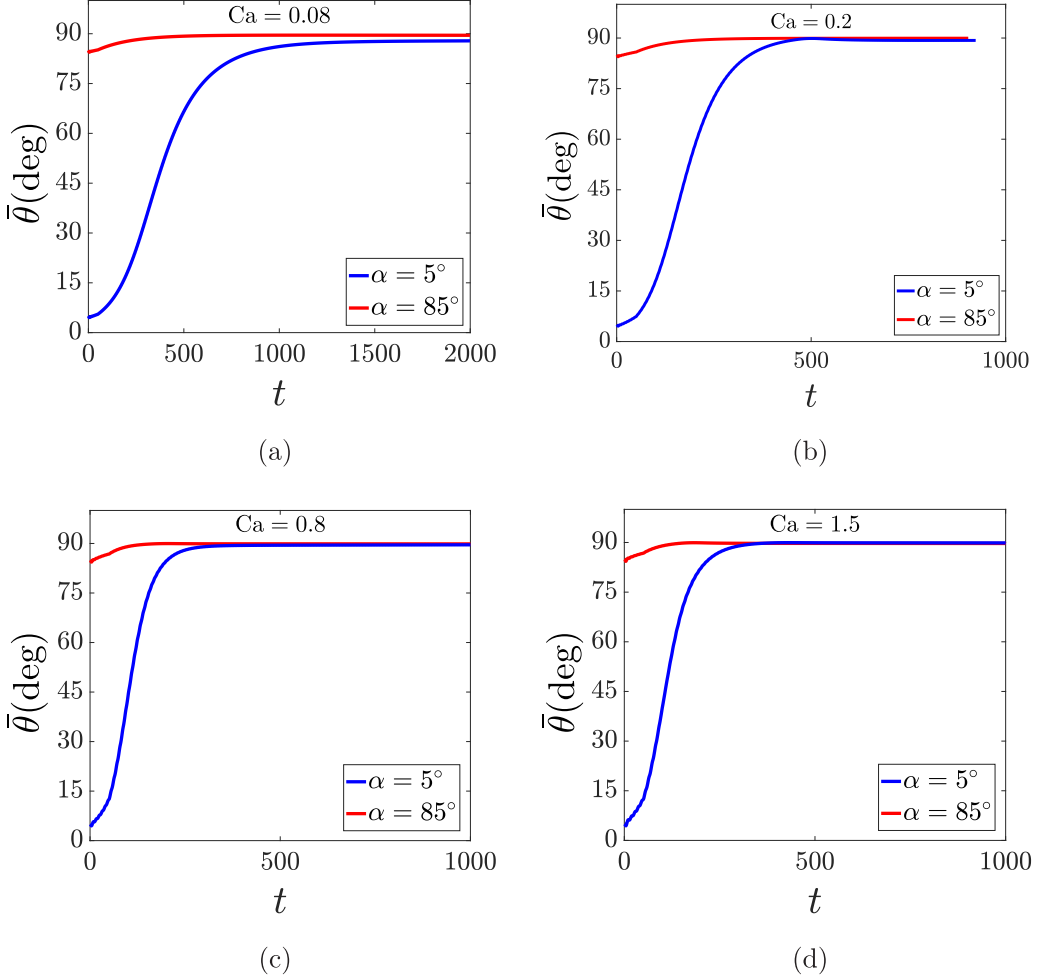
FIG. 7. Evolution of $\bar{\theta}$ of a prolate capsule (AR = 2.0) with $\hat{\kappa}_B = 0.2$ and $\lambda = 1$ at varying Ca. At low Ca the capsule takes a stable tumbling motion at long times [(a) Ca = 0.08 and (b) Ca = 0.2]. A tumbling-to-swinging transition is observed at moderate Ca [(c) Ca = 0.8] before swinging becomes the attractor at high Ca [(d) Ca = 1.5].

the orbital dynamics at increasing Ca from drift precession (the rolling regime) to stable precession accompanied by a tank-treading behavior of the membrane (the oscillating-swinging regime) for a prolate capsule (AR = 2.0, $\lambda = 1$) with zero spontaneous curvature and small bending stiffness ($\hat{\kappa}_B = 0.01$). These results suggest that the spontaneous curvature has a minor effect on the orbital behavior of the capsule.

Using Eq. (10), we can predict the rheology for a suspension of prolate capsules in the dilute limit. Figure 6 shows the capillary-number dependence of the time-averaged intrinsic viscosity and the dimensionless normal stress differences predicted for a dilute suspension of such capsules, all of which assume that same orbit for AR = 2.0 and $\hat{\kappa}_B = 0.02$. A decrease in the intrinsic viscosity [η] with increasing Ca, i.e., shear-thinning, is observed for all viscosity ratios considered here, and [η] decreases with increasing λ at each Ca [Fig. 6(a)]. Shear-thinning is the generally expected behavior for dilute suspensions of deformable particles, and indeed it has also been observed for dilute suspensions of other types of capsules, such as spherical capsules [12,38,39,42,43], oblate capsules [44], and biconcave discoidal capsules [40,41,45]. Results for the dimensionless normal
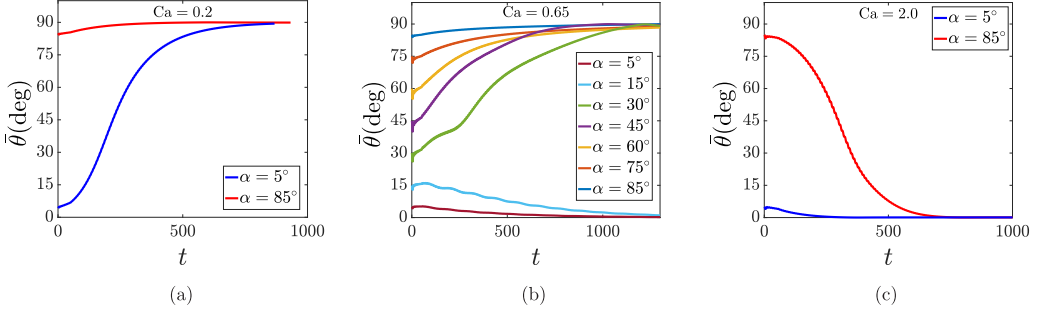
FIG. 8. Evolution of $\bar{\theta}$ of a prolate capsule (AR = 2.0) with $\hat{\kappa}_B = 0.2$ and $\lambda = 5$ at (a) Ca = 0.2, (b) Ca = 0.65, and (c) Ca = 2.0.

stress differences N_1 and N_2 are shown in Figs. 6(b) and 6(c), respectively. For all cases, $N_1 > 0$ and $N_2 < 0$, with $|N_2| \ll N_1$. In general, both N_1 and $|N_2|$ decrease with increasing λ at each Ca, and increase monotonically with Ca for $\lambda = 1.0$ and 0.2. For $\lambda = 5.0$, however, N_1 is observed to show a nonmonotonic dependency on Ca, while $|N_2|$ decreases with Ca.

B. Dynamics of prolate capsules with large bending stiffness

We found in the previous section that the long-time orbits for a prolate capsule with small bending stiffness are always independent of the initial conditions, although the stable orbital motions vary with capillary number. In this section, we investigate the dynamics of a prolate capsule with large bending stiffness. The spontaneous shape of the capsule is always assumed to be the same as its rest shape unless stated otherwise. We vary the viscosity ratio λ, capillary number Ca, initial orientation α, and aspect ratio AR of the capsule while keeping the bending modulus $\hat{\kappa}_B = 0.2$. We reveal that large bending stiffness coupled with high viscosity ratio can give rise to a multiplicity of attractors for the capsule dynamics, which will be presented and discussed below.

Again, we begin with $\lambda = 1$ and AR = 2.0. Unlike the case with $\hat{\kappa}_B = 0.02$, in this case the stable orbit for the capsule is always in the shear plane, as shown by the α-independent convergence of $\bar{\theta}$ toward $90°$ at varying Ca in Fig. 7. The time it takes for this transient convergence decreases in general with increasing Ca. This conclusion holds as λ decreases from 1 to 0.2, and also as AR increases from 2.0 to 3.0 (not shown). In a previous numerical study by Walter *et al.* [17], two regimes of stable orbital motion were found for a prolate capsule with the major axis initially lying in the shear plane: a rigid-body-like tumbling motion at low capillary number, and a fluidlike swinging motion at high shear rate, in which the capsule elongation and orientation both oscillate in shear flow with the membrane continuously rotating around its deformed shape. Here we observe similar dynamics. At low Ca, the capsule takes tumbling as the stable orbit [Figs. 7(a) and 7(b)], while at high Ca swinging becomes the attractor [Fig. 7(d)]; a tumbling-to-swinging transition is observed at moderate Ca [Fig. 7(c)], which is characterized by a nearly circular profile of the deformed capsule in the shear plane and roughly the same length of the two principal axes of the capsule during each half-period. A similar transition was also observed for a prolate solid elastic particle in shear flow in both a theoretical prediction by Gao *et al.* [59] and a numerical investigation by Villone *et al.* [60].

Now we consider the cases where the viscosity ratio λ is greater than unity. Figure 8 shows the evolution of $\bar{\theta}$ over time for a prolate capsule with AR = 2.0 and $\lambda = 5$ at varying Ca. At low and high Ca regimes, the orbit of the capsule converges toward $\bar{\theta}_{eq} = 90°$ and $0°$, representing a stable tumbling and rolling motion, respectively [Figs. 8(a) and 8(c)]. At intermediate Ca, however, the orbit taken by the capsule at long times is found to depend on the initial orientation, as observed in Fig. 8(b). Several values of α ranging from $5°$ to $85°$ are considered here to illustrate the dependence of the long-time orbit on the initial orientation, and the results for a range of Ca are displayed in Fig. 9. The key characteristic of this regime is that multiple stable orbits coexist, as observed in
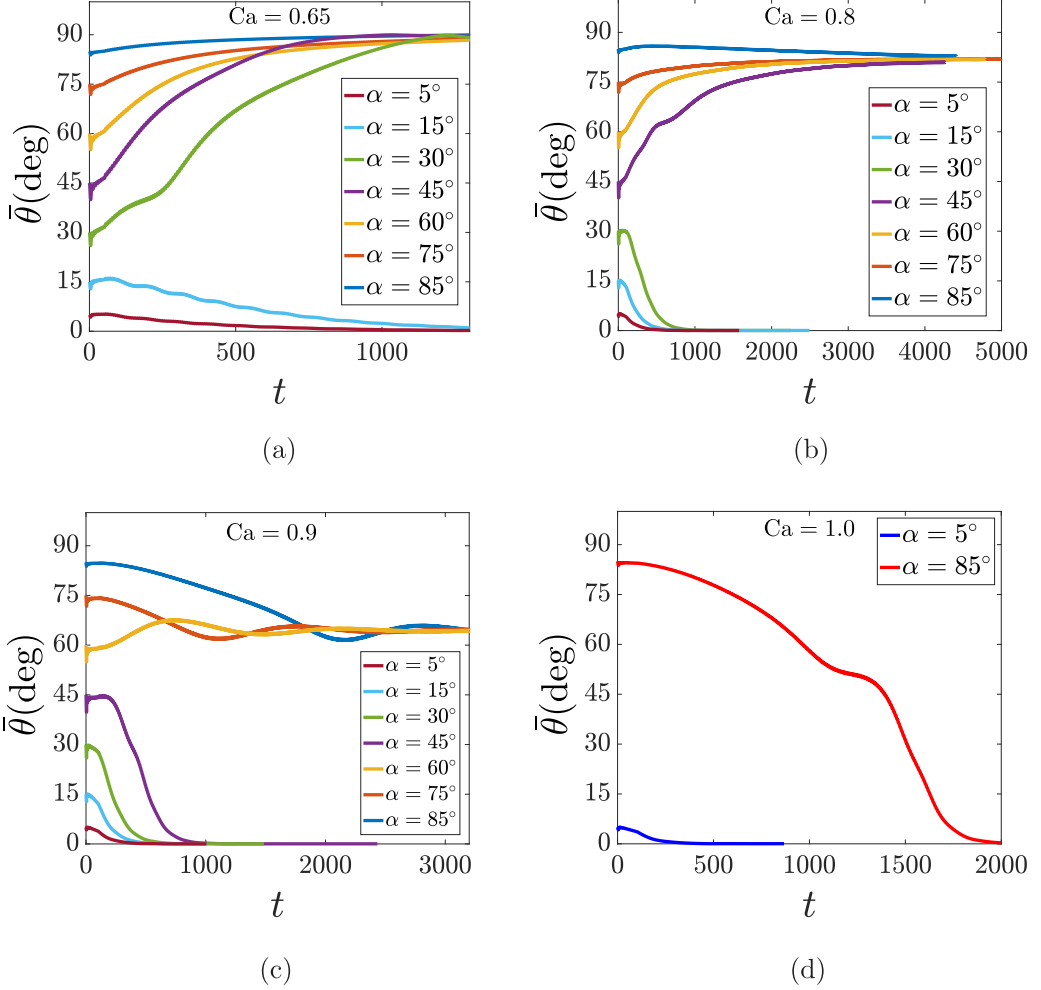
FIG. 9. Evolution of $\bar{\theta}$ of a prolate capsule (AR = 2.0) with $\hat{\kappa}_B = 0.2$ and $\lambda = 5$ at (a) Ca = 0.65, (b) Ca = 0.8, (c) Ca = 0.9, and (d) Ca = 1.0.

Figs. 9(a), 9(b) and 9(c). In this multiplicity regime, two stable solution branches are found as the capsule with varying α evolves toward the long-time orbit. The lower branch always corresponds to a stable rolling motion with $\bar{\theta}_{eq} = 0°$. For the upper branch, $\bar{\theta}_{eq}$ decreases with increasing Ca from $90°$, which corresponds to a stable tumbling motion, to intermediate values representing stable precessing motions about the shear plane. The multiplicity of attractors disappears as Ca further increases, and $\bar{\theta}_{eq} = 0°$ (rolling) becomes the only stable orbit [Fig. 9(d)]. Another important observation is that the critical value of α for the two branches of the evolution results, denoted as α_c, increases as Ca increases. Here it is not necessary to determine the exact values for α_c; actually, a range for α_c at each Ca is sufficient to show this trend: $\alpha_c \in (15°, 30°)$ at Ca = 0.65 [Fig. 9(a)], $\alpha_c \in (30°, 45°)$ at Ca = 0.8 [Fig. 9(b)], and $\alpha_c \in (45°, 60°)$ at Ca = 0.9 [Fig. 9(c)].

The global effects of Ca on $\bar{\theta}_{eq}$ for the attractors and α_c for the multiplicity regime described above are summarized as a bifurcation diagram in Fig. 10(a). The values for $\bar{\theta}_{eq}$ corresponding to the attractors in different regimes, either single or multiple, are represented by the solid blue lines with circles, and the estimated values for α_c by the dashed blue line with circles. Again, there are always solutions at $\theta = 0°$ and $90°$ that correspond to the orbits for a capsule aligned with the z axis
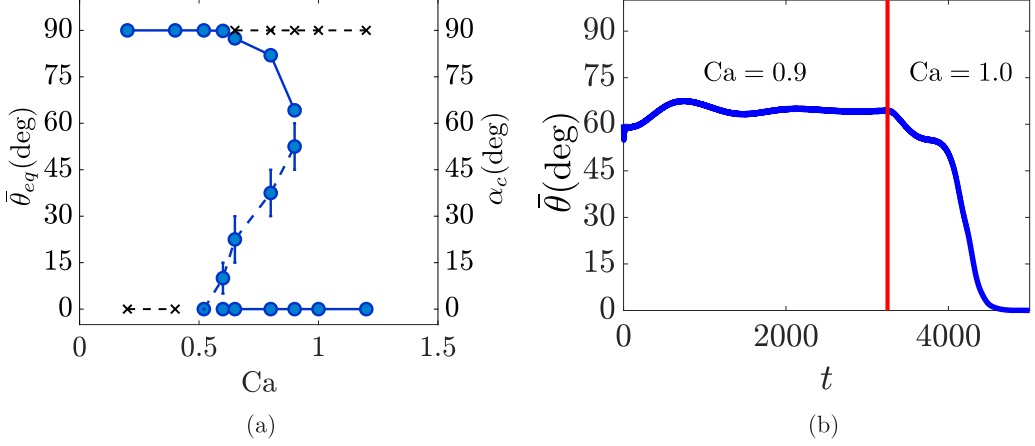
FIG. 10. (a) Bifurcation behavior for a prolate capsule (AR = 2.0) with $\hat{\kappa}_B = 0.2$ and $\lambda = 5$. The values for $\bar{\theta}_{\mathrm{eq}}$ corresponding to the attractors are represented by the solid blue lines with filled circles, and the estimated values for α_c by the dashed blue line with filled circles (the error bars indicating the range for α_c at each Ca in the multiplicity regime). The unstable solutions at $\theta = 0°$ and $90°$ are indicated by the dashed black lines with crosses. (b) Evolution of $\bar{\theta}$ for a capsule with $\alpha = 60°$ initially at Ca = 0.9. When a stable orbit is reached, the value of Ca is suddenly increased to 1.0, and the capsule evolves toward a new stable orbit.

and in the shear plane, respectively. These solutions are found to be unstable in certain regimes of Ca, as indicated by the dashed black lines with crosses. Indeed, there is a symmetry-breaking bifurcation away from $\theta = 90°$ between Ca = 0.6 and 0.65, and away from $\theta = 0°$ between Ca = 0.4 and 0.52. Two branches of attractors are observed. With any instantaneous orientation θ above the dashed blue line, the capsule would be attracted to a stable orbit on the upper branch of the attractors at the corresponding Ca, while any value for θ below the dashed blue line converges toward a rolling orbit on the lower branch with $\bar{\theta}_{\mathrm{eq}} = 0°$. The turning point at Ca ≈ 0.9 corresponds to a saddle-node bifurcation—for higher Ca this intermediate solution loses existence. This loss of existence is indicated by computing the solution at Ca = 0.9 and suddenly increasing Ca from 0.9 to 1.0 [Fig. 10(b)]. The capsule now evolves from a stable precession to a rolling motion as taken by a capsule with the same initial orientation initially at Ca = 1.0.

Similar to our findings, a tumbling-to-rolling transition was also observed for a prolate capsule (AR = 2.0, $\lambda = 1$) with zero bending resistance but in the presence of a small particle inertia [21], and a multiplicity of attractors was found in the transition regime. Other studies [61–63] have also reported a dependence of the stable orbit on the initial orientation for a solid prolate particle at certain Reynolds number regimes. A recent experimental investigation of red blood cells under shear flow in the dilute regime by Minetti *et al.* [64] has revealed hysteresis loops in the fraction of tank-treading cells upon increasing or decreasing shear rate. This result implies the presence of at least two populations of cells with different orbital dynamics that stably coexist in the same shear flow. This is exactly the situation that our computational results imply. Figure 11(a) shows the bifurcation behavior of the attractors for a prolate capsule ($\lambda = 5$) with various aspect ratios. It is observed that as AR increases from 2.0 to 3.0, the onset of the multiplicity regime occurs at a higher Ca, and this regime becomes broader. The effect of the viscosity ratio λ is illustrated in Fig. 11(b) for a capsule with AR = 3.0. In the parameter regime considered here, the multiplicity regime starts at a lower Ca and becomes narrower with increasing λ, showing an effect opposite to that of the aspect ratio. The orbital modes are determined for the attractors on the upper branch of the multiplicity, and summarized in a phase diagram over a wide range of Ca and λ [Fig. 11(c)]. Snapshots of a capsule ($\lambda = 6$) taking a stable tumbling, precessing, and rolling motion are shown in Figs. 12(a), 12(b), and 12(c), respectively, as examples.
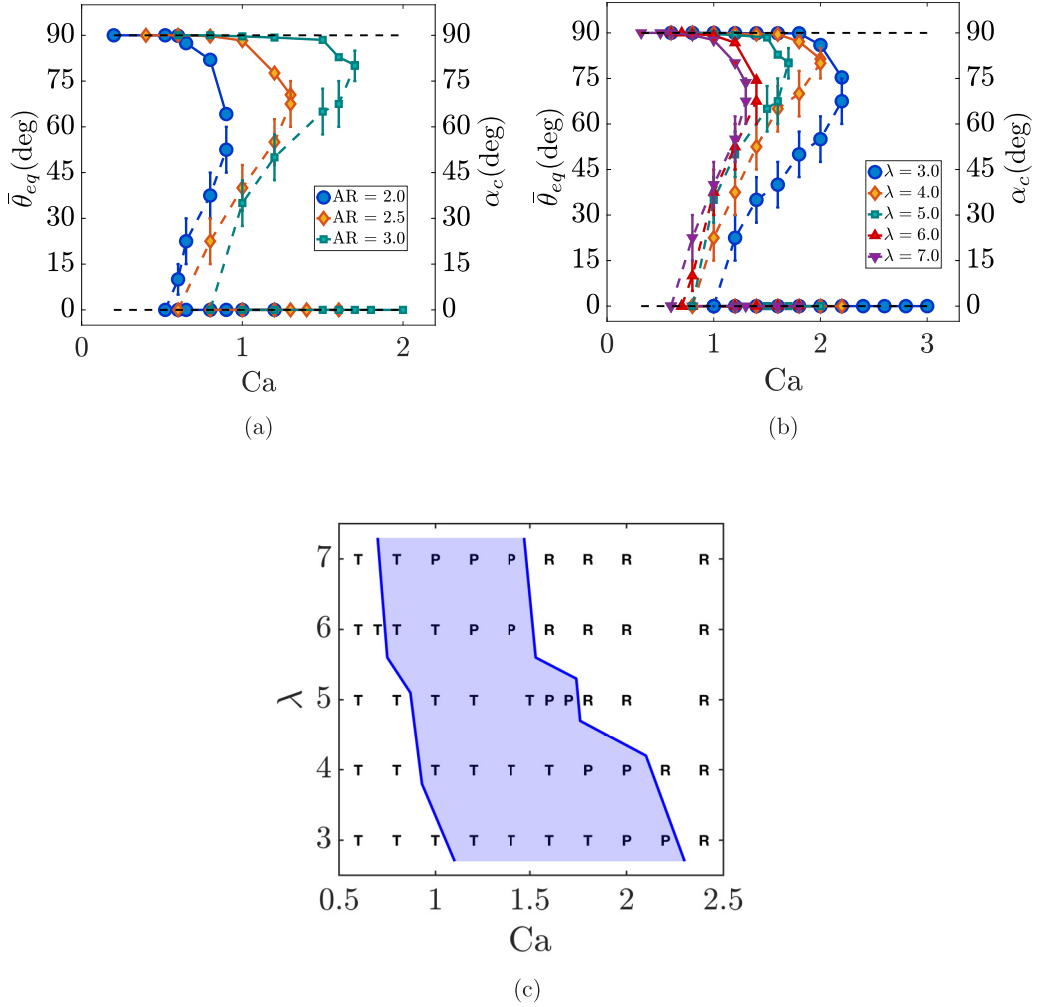
FIG. 11. Effects of capsule aspect ratio [(a) $\lambda = 5$] and the viscosity ratio [(b) AR = 3.0] on the bifurcation behavior of the attractors for a prolate capsule with $\hat{\kappa}_B = 0.2$. Again, the black dashed lines at $\theta = 0°$ and $90°$ correspond to the orbits for a capsule aligned with the z axis and in the shear plane, respectively. (c) Phase diagram of stable orbital motions for a prolate capsule (AR = 3.0) with $\hat{\kappa}_B = 0.2$ over a range of Ca and λ. The multiplicity regime is shaded in blue, and only the motion modes for the attractors on the upper branch are shown here (the attractors on the lower branch always correspond to rolling and thus are not shown here). T denotes tumbling, P precessing, and R rolling.

The multiplicity in attractors for a single prolate capsule, as described above, implies a multiplicity in the rheological properties for a dilute suspension of such capsules (AR = 3.0 and $\hat{\kappa}_B = 0.2$). Results are summarized in Fig. 13 for two viscosity ratios, $\lambda = 3.0$ and 5.0. For each λ, the squares represent the pure tumbling regime at lower Ca, while the circles represent the pure rolling regime at higher Ca; the multiplicity regime at intermediate Ca is bounded by vertical dotted lines, the downward and upward triangles representing the attractors on the upper branch (either tumbling or precessing) and the stable rolling orbits on the lower branch, respectively. All capsules are assumed to take the same stable orbit at each Ca. In this idealized situation, two different stable values for the particle stress can coexist when Ca is in the multiplicity regime. A general shear-thinning behavior is observed in Fig. 13(a) for both viscosity ratios, and minor differences
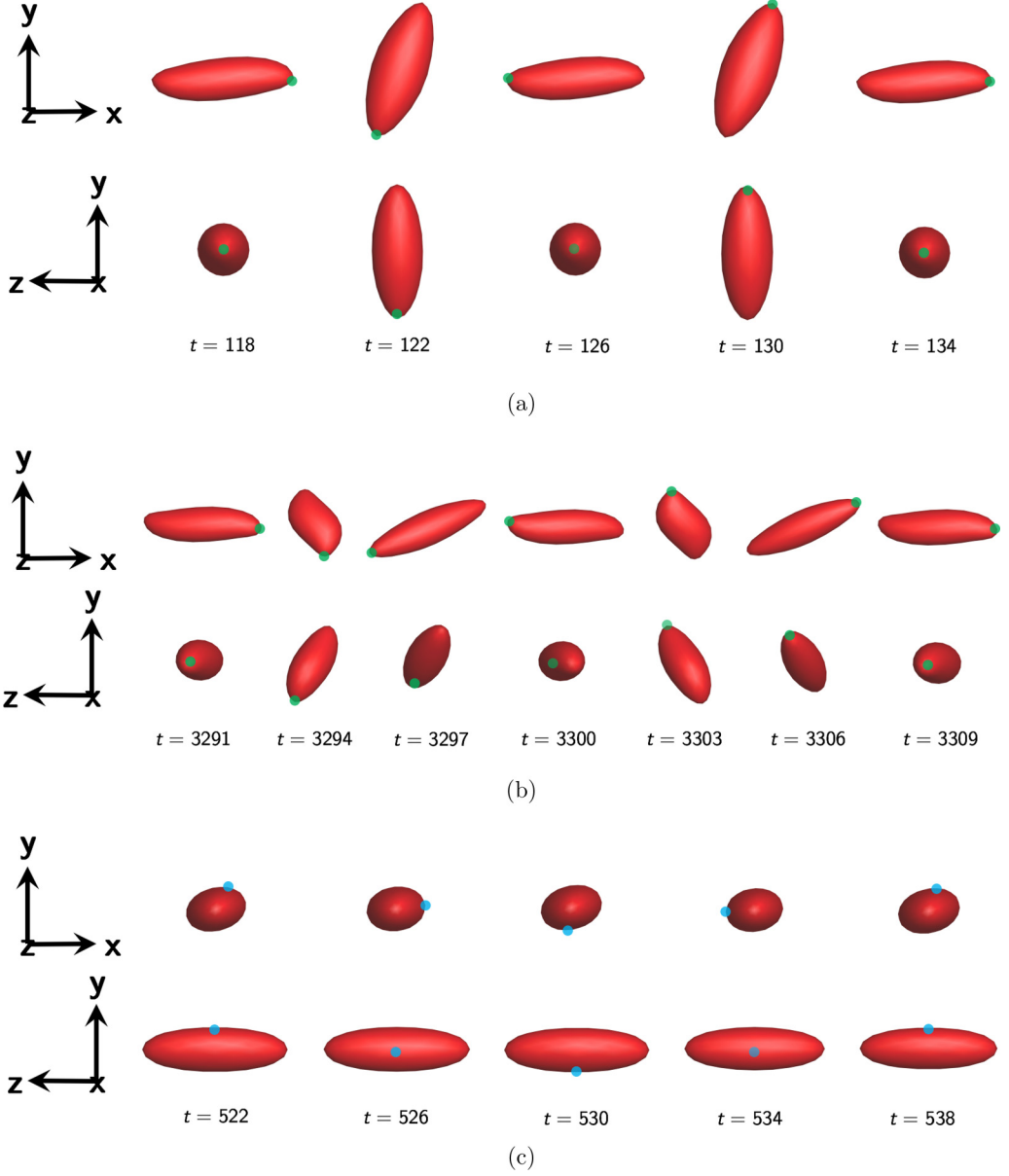
FIG. 12. Time sequence images (side and front views) of a prolate capsule (AR $= 3.0$) with $\hat{\kappa}_B = 0.2$ and $\lambda = 6.0$ taking a tumbling [(a) Ca $= 0.6$], precessing [(b) Ca $= 1.4$], and rolling [(c) Ca $= 2.0$] motion, respectively. The initial orientation of the capsule is $\alpha = 75°$. The markers indicate the positions of a membrane point initially on the major axis of the capsule for (a) and (b), and a membrane point initially on the equator of the capsule for (c).

are observed between these two cases. This shear-thinning behavior is also observed for $\lambda = 1.0$ and 0.2 (not shown). Another observation is that $[\eta]$ is higher when the capsules are taking a stable tumbling (or precessing) motion than it is when they are rolling. Mueller *et al.* [65] numerically determined the Einstein coefficient for a dilute suspension of inertialess nonspherical solid particles with a distribution of orientations, and reported similar findings: the contribution of a prolate particle
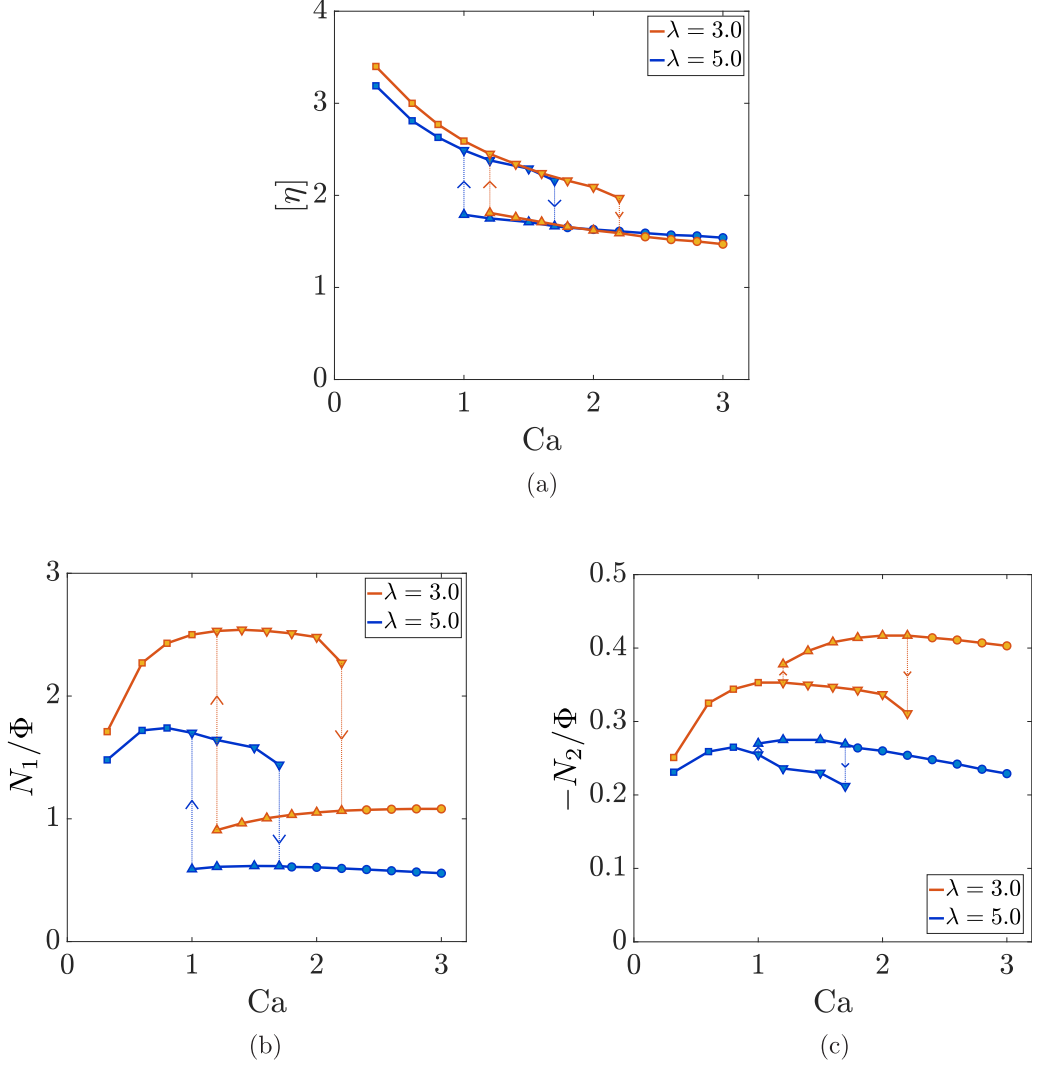
FIG. 13. Intrinsic viscosity (a) and dimensionless normal stress differences (b,c) predicted for a dilute suspension (with volume fraction Φ) of identical prolate capsules (AR = 3.0) with $\hat{\kappa}_B = 0.2$ taking the same corresponding stable orbit(s) at varying Ca for $\lambda = 3.0$ and 5.0. In each case, the squares represent the pure tumbling orbits at lower Ca, and the circles represent the pure rolling orbits at higher Ca; the downward and upward triangles represent the attractors on the upper branch (either tumbling or precessing) and the stable rolling orbits on the lower branch of the multiplicity regime (bounded by vertical dotted lines), respectively.

to the suspension viscosity (i.e., the *yx*-component of the particle's force dipole) decreases as the orbit of the capsule evolves from tumbling to rolling. Huang *et al.* [62] showed that this conclusion still holds in the presence of small inertia.

For the dimensionless normal stress differences N_1 and N_2 [Figs. 13(b) and 13(c)], again, the values are always positive for N_1 and negative for N_2, with $|N_2| \ll N_1$. Specifically, N_1 displays an obvious nonmonotonic dependency on Ca when the capsules are tumbling or precessing, while having smaller values and showing a small variation with Ca for a suspension of rolling capsules. This trend with Ca is qualitatively similar for both viscosity ratios, even though the magnitude of N_1 corresponding to each line is much smaller for the higher viscosity ratio ($\lambda = 5.0$).

A nonmonotonicity is also observed for N_2. Overall, as a result of the existence of the multiplicity regime, the values for each quantity of the rheology follow the path along the upper branch, and eventually fall onto the lower branch through the right vertical dotted line upon quasistatically increasing Ca; conversely, the values move along the lower branch and jump onto the upper branch via the left vertical dotted line upon quasistatically decreasing Ca. These processes are illustrated by the arrows in each figure of Fig. 13.

The presence of this complex rheological behavior naturally raises the question of whether there might be important fluid-mechanical consequences such as shear banding. In the dilute regime these phenomena cannot arise because the particle contribution to the total stress is much smaller than the stress due to the solvent, so the flow curve (shear stress versus strain rate) will not deviate substantially from linear. If the multiplicity were to persist to large concentration, the resulting flow curve is of the type that would lead not to shear banding (where two shear rates exist for the same shear stress) but to vorticity banding (where two shear stresses exist for the same shear rate) [66].

More generally, at finite concentration the particles are hydrodynamically coupled, which may result in changes to the dynamics. One natural question is whether the orbits of particles can become synchronized. While possible, we consider this unlikely, as while the particles are rotating, they are also moving past one another due to the mean shear and thus are only in close proximity for a timescale of a few strain units.

IV. CONCLUSION

In this work, we have systematically explored the orbital dynamics of an inertialess neutrally buoyant deformable prolate capsule in unbounded simple shear flow using direct simulations. For a capsule with small bending stiffness, we revealed that the orbit always converges toward a unique stable equilibrium state independent of the initial orientation. As Ca increases, the stable orbit evolves from the z (vorticity) axis to the shear plane. This trend holds qualitatively for all values of λ and AR considered in this study. Four dynamical modes for the stable orbit, namely rolling, wobbling, oscillating-swinging, and swinging, are determined at increasing Ca, similar to the findings by Dupont *et al.* [36]. The spontaneous curvature is shown to have a minor effect on the orbital dynamics of the capsule, although we believe that the artificial capsules in experiments are more likely to adopt a spontaneous shape the same as or close to the rest shape, instead of a flat sheet, which would lead to higher stress and strain energy in the membrane surface.

For a capsule with large bending stiffness, we found that the viscosity ratio λ plays a significant role in the determination of the stable orbits. When $\lambda \lesssim 1$, the stable orbit is always in the shear plane. Two regimes of stable orbital motions are identified: a rigid-body-like tumbling motion at low Ca, and a fluidlike swinging motion at high Ca. When $\lambda > 1$, the stable motion is tumbling and rolling at low and high Ca regimes, respectively, independent of the initial orientation. During the transition, however, the capsule is found to adopt multiple stable orbital modes including tumbling, precessing, and rolling, depending on the initial orientation. This multiplicity regime becomes broader as the aspect ratio of the capsule increases, while showing an opposite dependency on the viscosity ratio. We also predicted a general shear-thinning behavior and a multiplicity in the rheological properties for a dilute suspension of prolate capsules all assuming the same orbit, as a result of the multiplicity in the attractors for the capsule dynamics.

We note, though, that the membrane model adopted in this work has limitations. The model assumes that the capsule membrane is infinitely thin, while incorporating bending resistance by simply adding a bending energy cost function to account for the effect of the finite thickness of the capsule membrane. Such a decoupled energy-based model, as pointed out in a prior work by Dupont *et al.* [67], may be most suitable for particles with a composite membrane such as RBCs, which have a membrane comprising a fluid lipid bilayer tethered to an elastic spectrin network [68]. However, for artificial capsules that may likely have a homogeneous membrane with finite thickness, the accuracy of this model may need further investigation. In addition, the feasibility of this model in terms of describing large bending resistance of the membrane, as considered in this study, may

be questionable. Future works should examine the robustness of this model against other membrane models that consider nonzero thickness.

Overall, this work has revealed rich orbital dynamics for single prolate capsules in shear flow over a broad domain of parameter space, and illustrated how the stable orbits for a prolate capsule can be linked to the rheological properties for a suspension of such capsules in the dilute limit. We hope that these results will motivate experiments to probe the phenomenon of multiplicity of stable orbits predicted here.

[1] K. Alessandri, B. R. Sarangi, V. V. Gurchenkov, B. Sinha, T. R. Kießling, L. Fetler, F. Rico, S. Scheuring, C. Lamaze, A. Simon, S. Geraldo, D. Vignjević, H. Doméjean, L. Rolland, A. Funfak, J. Bibette, N. Bremond, and P. Nassoy, Cellular capsules as a tool for multicellular spheroid production and for investigating the mechanics of tumor progression in vitro, Proc. Natl. Acad. Sci. (USA) **110**, 14843 (2013).

[2] F. Casanova and L. Santos, Encapsulation of cosmetic active ingredients for topical application—A review, J. Microencapsul. **33**, 1 (2016).

[3] K. Masuda, Development of a drug delivery system using microcapsules with ultrasound, Biocybern. Biomed. Eng. **31**, 23 (2011).

[4] P. Degen, Self-propelling capsules as artificial microswimmers, Curr. Opin. Colloid Interface Sci. **19**, 611 (2014).

[5] D. A. Jones, J. G. Munford, and P. A. Gabbott, Microcapsules as artificial food particles for aquatic filter feeders, Nature (London) **247**, 233 (1974).

[6] B. G. De Geest, N. N. Sanders, G. B. Sukhorukov, J. Demeester, and S. C. De Smedt, Release mechanisms for polyelectrolyte capsules, Chem. Soc. Rev. **36**, 636 (2007).

[7] Y. Geng, P. Dalhaimer, S. Cai, R. Tsai, M. Tewari, T. Minko, and D. E. Discher, Shape effects of filaments versus spherical particles in flow and drug delivery, Nat. Nanotechnol. **2**, 249 (2007).

[8] J. A. Champion and S. Mitragotri, Shape induced inhibition of phagocytosis of polymer particles, Pharm. Res. **26**, 244 (2009).

[9] X. Zan, A. Garapaty, and J. A. Champion, Engineering polyelectrolyte capsules with independently controlled size and shape, Langmuir **31**, 7601 (2015).

[10] I. Schneeweiss and H. Rehage, Non-spherical capsules for the food industry, Chem. Ing. Tech. **77**, 236 (2005).

[11] D. Barthès-Biesel and J. M. Rallison, The time-dependent deformation of a capsule freely suspended in a linear shear flow, J. Fluid Mech. **113**, 251 (1981).

[12] S. Ramanujan and C. Pozrikidis, Deformation of liquid capsules enclosed by elastic membranes in simple shear flow: Large deformations and the effect of fluid viscosities, J. Fluid Mech. **361**, 117 (1998).

[13] Y. Sui, H. T. Low, Y. T. Chew, and P. Roy, Tank-treading, swinging, and tumbling of liquid-filled elastic capsules in shear flow, Phys. Rev. E **77**, 016310 (2008).

[14] S. Kessler, R. Finken, and U. Seifert, Swinging and tumbling of elastic capsules in shear flow, J. Fluid Mech. **605**, 207 (2008).

[15] P. Bagchi and R. M. Kalluri, Dynamics of nonspherical capsules in shear flow, Phys. Rev. E **80**, 016307 (2009).

[16] D.-V. Le and Z. Tan, Large deformation of liquid capsules enclosed by thin shells immersed in the fluid, J. Comput. Phys. **229**, 4097 (2010).

[17] J. Walter, A. Salsac, and D. Barthès-Biesel, Ellipsoidal capsules in simple shear flow: Prolate versus oblate initial shapes, J. Fluid Mech. **676**, 318 (2011).

[18] A. Z. K. Yazdani, R. M. Kalluri, and P. Bagchi, Tank-treading and tumbling frequencies of capsules and red blood cells, Phys. Rev. E **83**, 046305 (2011).

[19] T. Omori, Y. Imai, T. Yamaguchi, and T. Ishikawa, Reorientation of a Nonspherical Capsule in Creeping Shear Flow, Phys. Rev. Lett. **108**, 138102 (2012).

[20] D. Cordasco and P. Bagchi, Orbital drift of capsules and red blood cells in shear flow, Phys. Fluids **25**, 091902 (2013).

[21] Z. Wang, Y. Sui, P. D. M. Spelt, and W. Wang, Three-dimensional dynamics of oblate and prolate capsules in shear flow, Phys. Rev. E **88**, 053021 (2013).

[22] C. Dupont, F. Delahaye, D. Barthès-Biesel, and A.-V. Salsac, Stable equilibrium configurations of an oblate capsule in simple shear flow, J. Fluid Mech. **791**, 738 (2016).

[23] H. L. Goldsmith, J. Marlow, and F. C. MacIntosh, Flow behavior of erythrocytes. I. Rotation and deformation in dilute suspensions, Proc. R. Soc. London B **182**, 351 (1972).

[24] T. Fischer, M. Stohr-Lissen, and H. Schmid-Schonbein, The red cell as a fluid droplet: Tank tread-like motion of the human erythrocyte membrane in shear flow, Science **202**, 894 (1978).

[25] M. Abkarian, M. Faivre, and A. Viallat, Swinging of Red Blood Cells Under Shear Flow, Phys. Rev. Lett. **98**, 188302 (2007).

[26] J. M. Skotheim and T. W. Secomb, Red Blood Cells and Other Nonspherical Capsules in Shear Flow: Oscillatory Dynamics and the Tank-Treading-to-Tumbling Transition, Phys. Rev. Lett. **98**, 078301 (2007).

[27] J. Dupire, M. Abkarian, and A. Viallat, Chaotic Dynamics of Red Blood Cells in a Sinusoidal Flow, Phys. Rev. Lett. **104**, 168101 (2010).

[28] D. A. Fedosov, B. Caswell, and G. E. Karniadakis, A multiscale red blood cell model with accurate mechanics, rheology, and dynamics, Biophys. J. **98**, 2215 (2010).

[29] D. A. Fedosov, H. Lei, B. Caswell, S. Suresh, and G. E. Karniadakis, Multiscale modeling of red blood cell mechanics and blood flow in malaria, PLoS Comput. Biol. **7**, e1002270 (2011).

[30] Z. Peng, R. J. Asaro, and Q. Zhu, Multiscale modeling of erythrocytes in Stokes flow, J. Fluid Mech. **686**, 299 (2011).

[31] A. Z. K. Yazdani and P. Bagchi, Phase diagram and breathing dynamics of a single red blood cell and a biconcave capsule in dilute shear flow, Phys. Rev. E **84**, 026314 (2011).

[32] J. Dupire, M. Socol, and A. Viallat, Full dynamics of a red blood cell in shear flow, Proc. Natl. Acad. Sci. (USA) **109**, 20808 (2012).

[33] D. Cordasco, A. Yazdani, and P. Bagchi, Comparison of erythrocyte dynamics in shear flow under different stress-free configurations, Phys. Fluids **26**, 041902 (2014).

[34] Z. Peng, A. Mashayekh, and Q. Zhu, Erythrocyte responses in low-shear-rate flows: Effects of non-biconcave stress-free state in the cytoskeleton, J. Fluid Mech. **742**, 96 (2014).

[35] K. Sinha and M. D. Graham, Dynamics of a single red blood cell in simple shear flow, Phys. Rev. E **92**, 042710 (2015).

[36] C. Dupont, A. Salsac, and D. Barthès-Biesel, Off-plane motion of a prolate capsule in shear flow, J. Fluid Mech. **721**, 180 (2013).

[37] R. Skalak, A. Tozeren, R. P. Zarda, and S. Chien, Strain energy function of red blood-cell membranes, Biophys. J. **13**, 245 (1973).

[38] D. Barthès-Biesel and V. Chhim, The constitutive equation of a dilute suspension of spherical microcapsules, Int. J. Multiph. Flow **7**, 493 (1981).

[39] C. Pozrikidis, Finite deformation of liquid capsules enclosed by elastic membranes in simple shear flow, J. Fluid Mech. **297**, 123 (1995).

[40] C. Pozrikidis, Numerical simulation of the flow-induced deformation of red blood cells, Ann. Biomed. Eng. **31**, 1194 (2003).

[41] A. Drochon, Rheology of dilute suspensions of red blood cells: Experimental and theoretical approaches, Eur. Phys. J. AP **22**, 155 (2003).

[42] P. Bagchi and R. M. Kalluri, Rheology of a dilute suspension of liquid-filled elastic capsules, Phys. Rev. E **81**, 056320 (2010).

[43] J. R. Clausen and C. K. Aidun, Capsule dynamics and rheology in shear flow: Particle pressure and normal stress, Phys. Fluids **22**, 123302 (2010).

[44] P. Bagchi and R. M. Kalluri, Dynamic rheology of a dilute suspension of elastic capsules: Effect of capsule tank-treading, swinging and tumbling, J. Fluid Mech. **669**, 498 (2011).

[45] N. Takeishi, M. E. Rosti, Y. Imai, S. Wada, and L. Brandt, Haemorheology in dilute, semi-dilute and dense suspensions of red blood cells, J. Fluid Mech. **872**, 818 (2019).

[46] G. B. Jeffery, The motion of ellipsoidal particles immersed in a viscous fluid, Proc. R. Soc. London A **102**, 161 (1922).

[47] P. B. Canham, The minimum energy of bending as a possible explanation of the biconcave shape of the human red blood cell, J. Theor. Biol. **26**, 61 (1970).

[48] W. Helfrich, Elastic properties of lipid bilayers: Theory and possible experiments, Z. Naturforsch. C **28**, 693 (1973).

[49] D. Barthès-Biesel, A. Diaz, and E. Dhenin, Effect of constitutive laws for two-dimensional membranes on flow-induced capsule deformation, J. Fluid Mech. **460**, 211 (2002).

[50] A. Kumar and M. D. Graham, Accelerated boundary integral method for multiphase flow in non-periodic geometries, J. Comput. Phys. **231**, 6682 (2012).

[51] J. Charrier, S. Shrivastava, and R. Wu, Free and constrained inflation of elastic membranes in relation to thermoforming—Non-axisymmetric problems, J. Strain Anal. Eng. Des. **24**, 55 (1989).

[52] M. Meyer, M. Desbrun, P. Schröder, and A. H. Barr, Discrete differential geometry operators for triangulated 2-manifolds, in *Visualization and Mathematics III, Mathematics and Visualization* (Springer, Berlin, 2003), pp. 35–57.

[53] C. Pozrikidis, *Boundary Integral and Singularity Methods for Linearized Viscous Flow*, Cambridge Texts in Applied Mathematics (Cambridge University Press, Cambridge, 1992).

[54] X. Zhang, W. A. Lam, and M. D. Graham, Dynamics of deformable straight and curved prolate capsules in simple shear flow, Phys. Rev. Fluids **4**, 043103 (2019).

[55] G. K. Batchelor, The stress system in a suspension of force-free particles, J. Fluid Mech. **41**, 545 (1970).

[56] M. R. Kennedy, C. Pozrikidis, and R. Skalak, Motion and deformation of liquid drops, and the rheology of dilute emulsions in simple shear flow, Comput. Fluids **23**, 251 (1994).

[57] M. D. Graham, *Microhydrodynamics, Brownian Motion, and Complex Fluids*, Cambridge Texts in Applied Mathematics (Cambridge University Press, Cambridge, 2018).

[58] A. Einstein, Berichtigung zu meiner arbeit: "Eine neue bestimmung der moleküldimensionen", Ann. Phys. **339**, 591 (1911).

[59] T. Gao, H. H. Hu, and P. P. Castañeda, Shape Dynamics and Rheology of Soft Elastic Particles in a Shear Flow, Phys. Rev. Lett. **108**, 058302 (2012).

[60] M. M. Villone, G. D'Avino, M. A. Hulsen, and P. L. Maffettone, Dynamics of prolate spheroidal elastic particles in confined shear flow, Phys. Rev. E **92**, 062303 (2015).

[61] Z. Yu, N. Phan-Thien, and R. I. Tanner, Rotation of a spheroid in a Couette flow at moderate Reynolds numbers, Phys. Rev. E **76**, 026310 (2007).

[62] H. Huang, X. Yang, M. Krafczyk, and X.-Y. Lu, Rotation of spheroidal particles in Couette flows, J. Fluid Mech. **692**, 369 (2012).

[63] T. Rosen, F. Lundell, and C. K. Aidun, Effect of fluid inertia on the dynamics and scaling of neutrally buoyant particles in shear flow, J. Fluid Mech. **738**, 563 (2014).

[64] C. Minetti, V. Audemar, T. Podgorski, and G. Coupier, Dynamics of a large population of red blood cells under shear flow, J. Fluid Mech. **864**, 408 (2019).

[65] S. Mueller, E. W. Llewellin, and H. M. Mader, The rheology of suspensions of solid particles, Proc. R. Soc. London A **466**, 1201 (2010).

[66] J. K. G. Dhont and W. J. Briels, Gradient and vorticity banding, Rheol. Acta **47**, 257 (2008).

[67] C. Dupont, A.-V. Salsac, D. Barthès-Biesel, M. Vidrascu, and P. Le Tallec, Influence of bending resistance on the dynamics of a spherical capsule in shear flow, Phys. Fluids **27**, 051902 (2015).

[68] N. Mohandas and E. Evans, Mechanical properties of the red cell membrane in relation to molecular structure and genetic defects, Annu. Rev. Biophys. Biomol. Struct. **23**, 787 (1994).